Notes on Numerical Fluid Mechanics
and Multidisciplinary Design 132

Andreas Dillmann
Gerd Heller
Ewald Krämer
Claus Wagner
Christian Breitsamter *Editors*

New Results in Numerical and Experimental Fluid Mechanics X

Contributions to the 19th STAB/DGLR Symposium Munich, Germany, 2014

Springer

Notes on Numerical Fluid Mechanics and Multidisciplinary Design

Volume 132

About this Series

Notes on Numerical Fluid Mechanics and Multidisciplinary Design publishes state-of-art methods (including high performance methods) for numerical fluid mechanics, numerical simulation and multidisciplinary design optimization. The series includes proceedings of specialized conferences and workshops, as well as relevant project reports and monographs.

More information about this series at http://www.springer.com/series/4629

Andreas Dillmann · Gerd Heller
Ewald Krämer · Claus Wagner
Christian Breitsamter
Editors

New Results in Numerical and Experimental Fluid Mechanics X

Contributions to the 19th STAB/DGLR Symposium Munich, Germany, 2014

Springer

Editors
Andreas Dillmann
Deutsches Zentrum für Luft- und Raumfahrt
Institut für Aerodynamik und Strömungstechnik
Göttingen
Germany

Gerd Heller
Airbus Deutschland
Bremen
Germany

Ewald Krämer
Institut für Aerodynamik und Gasdynamik
Universität Stuttgart
Stuttgart
Germany

Claus Wagner
Deutsches Zentrum für Luft- und Raumfahrt
Institut für Aerodynamik und Strömungstechnik
Göttingen
Germany

Christian Breitsamter
Lehrstuhl für Aerodynamik und Strömungsmechanik
Technische Universität München
Garching
Germany

ISSN 1612-2909 ISSN 1860-0824 (electronic)
Notes on Numerical Fluid Mechanics and Multidisciplinary Design
ISBN 978-3-319-27278-8 ISBN 978-3-319-27279-5 (eBook)
DOI 10.1007/978-3-319-27279-5

Library of Congress Control Number: 2015958857

Printed on acid-free paper

This Springer imprint is published by SpringerNature
The registered company is Springer International Publishing AG Switzerland

Preface

This volume contains the papers presented at the 19th DGLR/STAB-Symposium held in Munich, Germany, 4–5 November 2014 and organized by the Institute of Aerodynamics and Fluid Mechanics of the Technische Universität München. STAB is the German Aerospace Aerodynamics Association, founded towards the end of the 1970s and DGLR is the German Society for Aeronautics and Astronautics (Deutsche Gesellschaft für Luft- und Raumfahrt - Lilienthal Oberth e.V.).

The mission of STAB is to foster development and acceptance of the disciplines "Aerodynamics and Fluid Mechnics" in Germany. One of its general guidelines is to concentrate resources and know-how in the involved institutions and to avoid duplication in research work as much as possible. Nowadays, this is more necessary than ever. The experience made in the past makes it easier now to obtain new knowledge for solving today's and tomorrow's problems. STAB unites German scientists and engineers from universities, research establishments and industry doing research and project work in numerical and experimental fluid mechanics and aerodynamics for aerospace, ground transportation and other applications. This has always been the basis of numerous common research activities sponsored by different funding agencies.

Since 1986 the symposium has taken place at different locations in Germany every 2 years. In between, STAB workshops regularly take place at the DLR in Göttingen. The changing meeting places were established as focal points in Germany's Aerospace Fluid Mechanics Community for a continuous exchange of scientific results and their discussion. Moreover, they are a forum where new research activities can be presented, often resulting in new, commonly organized research and technology projects.

It is the tenth time that the contributions to the symposium are published after being subjected to a peer review. The material highlights the key items of integrated research and development based on fruitful collaboration of industry, research establishments and universities. The research areas include airplane and ground vehicle aerodynamics, multidisciplinary optimization and new configurations, turbulence research and modelling, laminar flow control and transition, rotorcraft

aerodynamics, aeroelasticity and structural dynamics, numerical and experimental simulation including test techniques, aeroacoustics as well as biomedical and convective flows.

From some 94 lectures presented at the symposium, 77 are included in this book.

The Review-Board, partly identical with the Program-Committee, consisted of G. Axtmann (Stuttgart), M. Blechschmidt (München), J. Blinstrub (Göttingen), T. Böck (Ilmenau), F. Boden (Göttingen), S. Bogdanski (Stuttgart), J. Bosbach (Göttingen), J. Boschung (Aachen), S. Braun (Aachen), C. Breitsamter (München), M. Brüderlin (Aachen), M. Bruse (Göttingen), N. Buchmann (Braunschweig), M. Burnazzi (Braunschweig), M. Costantini (Göttingen), M. Costes (Frankreich), A. Dannhauer (Göttingen), R. Deiterding (Göttingen), J. Dierke (Braunschweig), A. Dillmann (Göttingen), P. Dörr (Stuttgart), T. Eggers (Braunschweig), K. Ehrenfried (Göttingen), D. Feldmann (Göttingen), U. Fey (Göttingen), H. Foysi (Siegen), M. Fragner (Göttingen), D. Franke (Braunschweig), D. Freudenhammer (Darmstadt), U. Füllekrug (Göttingen), M. Gageik (Aachen), A. Gardner (Göttingen), M. Gauding (Freiburg), S. Geisbauer (Braunschweig), C. Grabe (Göttingen), M. Grawunder (München), S. Grundmann (Darmstadt), J. Haff (Göttingen), V. Hannemann (Göttingen), R. Hartmann (Braunschweig), F. Haucke (Berlin), S. Hein (Göttingen), A. Henning (Göttingen), S. Hickel (München), R. Höld (Schrobenhausen), C. Ilic (Braunschweig), M. Jacobs (Göttingen), S. Jakirlic (Darmstadt), D. Jakubek (Göttingen), C. Kaiser (Göttingen), K. Kaufmann (Göttingen), A. Kerr (Göttingen), R. Kessler (Göttingen), N. Kin (Göttingen), T. Kirmse (Göttingen), C. Klein (Göttingen), I. Klioutchnikov (Aachen), M. Kloker (Stuttgart), T. Knopp (Göttingen), B. König (Stuttgart), M. Konstantinov (Göttingen), M. Körner (Ilmenau), T. Köthe (Göttingen), L. Krenkel (Regensburg), H. Kreplin (Göttingen), N. Kroll (Braunschweig), W. Krüger (Göttingen), A. Krumbein (Göttingen), A. Küpper (Braunschweig), H. Kurz (Stuttgart), L. Kutej (Darmstadt), S. Langer (Braunschweig), A. Länger (Braunschweig), M. Lühmann (Hamburg), T. Lutz (Stuttgart), M. Meinke (Aachen), A. Nemilie (Kaiserslautern), J. Neumann (Göttingen), H. Olivier (Aachen), M. Onur Cetin (Aachen), R. Placzek (Braunschweig), A. Pogorelov (Aachen), W. Polifke (München), M. Raffel (Göttingen), M. Rein (Göttingen), R. Reß (München), S. Reuß (Göttingen), K. Richter (Göttingen), S. Risius (Göttingen), U. Rist (Stuttgart), M. Rösler (Dresden), K. Rossignol (Braunschweig), C. Rossow (Braunschweig), D. Schicker (München), D. Schiepel (Göttingen), T. Schilden (Aachen), S. Schmidt (Hamburg), O. Schmidt (Stuttgart), R. Schnell (Köln), P. Scholz (Braunschweig), D. Schönweitz (Köln), A. Schröder (Göttingen), E. Schülein (Göttingen), R. Schuster (Göttingen), W. Send (Göttingen), B. Simon (Darmstadt), C. Sovardi (München), M. Springer (Erlangen), B. Stövesandt (Oldenburg), R. Streblow (Dresden), A. Stück (Braunschweig), A. Theiß (Göttingen), C. Voß (Göttingen), C. Wagner (Göttingen), S. Wagner (Göttingen), K. Weinman (Göttingen), J. Wendisch (Braunschweig), A. Westhoff (Göttingen), M. Wetzel (München), A. Wick (Hamburg), F. Wienke (Göttingen), J. Wild (Braunschweig), M. Winter (München), C. Zwerger (München).

Nevertheless, the authors sign responsible for the contents of their contributions.

The editors are grateful to Prof. Dr. W. Schröder as the General Editor of the "Notes on Numerical Fluid Mechanics and Multidisciplinary Design" and to the Springer-Verlag for the opportunity to publish the results of the symposium.

Göttingen — Andreas Dillmann
Bremen — Gerd Heller
Stuttgart — Ewald Krämer
Göttingen — Claus Wagner
München — Christian Breitsamter
July 2015

Contents

Part VIII Aeroelasticity and Structural Dynamics

Part IX Numerical Simulation / Aerodynamics

Part XI Aeroacoustics

Part I
Airplane Aerodynamics/Propulsion Integration

Numerical Stall Behavior Investigation of an Aircraft Equipped with Coanda Flap and Droop Nose

Marco Burnazzi, Jakob Thiemeier and Rolf Radespiel

Abstract An active high-lift set up is employed on a wing-body aircraft configuration and the stall behavior is analyzed by means of CFD RANS simulations. The high-lift system is composed of a trailing-edge gap-less Coanda flap and a leading-edge flexible droop nose. The effect of the leading-edge device is studied by using comparisons with the cruise leading-edge configuration. Comparisons with previous 2D simulations highlight lower lift performances for the wing section of the 3D model with respect to the airfoil data. This is due to 3D flow dynamics that limit the lift generated by the wing and induce stall with mechanisms not observed in 2D. Cross flow at the wing leading edge, or over the suction side of the wing root, increase the boundary layer thickness over the wing, thus reducing the efficiency of the Coanda flap.

1 Introduction

The low flight speed performance of an aircraft defines its capability to access airports with short runways. Flight speed is also an important factor in the emission of airframe noise. The commercial use of airports in the proximity of populated areas is an enabler for providing efficient point-to-point air travel connections. This approach represents a viable path to reducing noise emissions, fuel consumption and air traffic congestion. In this context a technological challenge is the high-lift system, as it allows for low flight speeds and is a major source of aircraft noise during landing. Both aspects can be successfully addressed by exploiting the potentials of active circulation control.

M. Burnazzi (✉) · J. Thiemeier · R. Radespiel
Technische Universität Braunschweig - Institut für Strömungsmechanik,
Hermann-Blenk-Straße 37, 38108 Braunschweig, Germany
e-mail: m.burnazzi@tu-bs.de

J. Thiemeier
e-mail: jakob.thiemeier@gmx.de

R. Radespiel
e-mail: r.radespiel@tu-bs.de

A. Dillmann et al. (eds.), *New Results in Numerical and Experimental Fluid Mechanics X*, Notes on Numerical Fluid Mechanics and Multidisciplinary Design 132, DOI 10.1007/978-3-319-27279-5_1

The active control of boundary-layer separation makes it possible to reach high lift targets without employing gaps from the lower wing surface to the upper, which were identified as the major source of noise from conventional high-lift devices [1]. The efficacy of controlling the behavior of the flow around an object by actively altering the boundary layer momentum was already demonstrated by Prandtl in 1927 [2]. Since then, a large variety of flow control techniques has been developed, assessing the potential of active circulation control for improving the aerodynamic performance parameters of wing airfoils [3–5]. However, the excessive power needed to prevent flow separation is still a major problem for the integration of the active high-lift system into an aircraft. For this reason, the current research on active high-lift systems puts considerable efforts on suited means to reduce momentum and hence, power required to obtain a given lift target. Furthermore, active flow control can yield very large amounts of circulation, which can cause unexpected flow behavior if the system is employed on a conventional aircraft configuration. These flow phenomena may limit the efficiency of the active system and increase power consumption. The analysis of such three-dimensional flow mechanisms is the main objective of the present work that describes the integration of an active high-lift configuration on a 3D wing-body aircraft model.

The active high-lift configuration investigated here is based on a Coanda flap. A thin air jet is tangentially blown over the suction side of a deflected simple-hinged flap, avoiding flow separation and achieving effective flow turning. This device yields very high circulation around the airfoil, creating the need for a leading edge device that can reduce the suction peak at the leading edge and increase the stall angle of attack. For this purpose the leading edge of the current configuration is equipped with a flexible droop nose device. This configuration was designed and extensively tested with 2D simulations, proving its high efficiency [6]. However, from 3D flow simulations some unexpected flow phenomena emerged, which limit the maximum lift and cause stall at angles of attack significantly lower than for the 2D analyses. Boundary layer cross flow at the leading edge and on the suction side of the wing root were identified as main causes of the lower performances in the 3D case. The discussion of these flow behaviors yields physical understanding of the integration aspects of an active high-lift device, and represents a valuable starting point for future developments of this technology.

2 High-Lift Configuration

The DLR F15 airfoil was modified to obtain an effective active high-lift configuration, as shown in Fig. 1. The high-lift configuration consists of two elements, the Coanda trailing edge flap and the droop-nose leading edge device.

The following sections briefly summarize the previous work that was undertaken to design the two devices, describing the starting point of the present project.

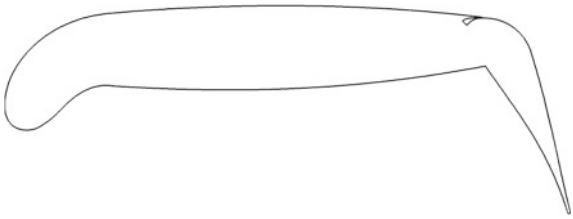

Fig. 1 High-lift configuration employed on the 3D model

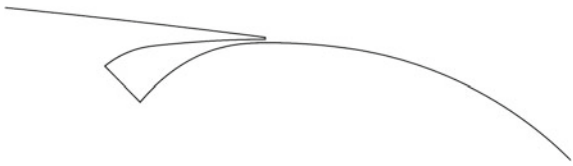

Fig. 2 Close-up of the blowing slot

2.1 Trailing-Edge Device

Previous numerical and experimental investigations aimed at reducing the momentum requirements of the Coanda flap by careful adjustments of the trailing edge design parameters, while the leading edge was geometrically fixed in cruise configuration. These initial design studies assumed steady blowing tangential to the flap surface to produce suited turbulent wall jets that exploit the Coanda effect for effective flow turning. The results indicated that the most important design parameters are the flap deflection angle, the blowing momentum coefficient, C_μ, and the blowing slot height [7]. Whereas flap angle and blowing momentum coefficient should increase for increased lift targets, slot heights remain rather small, with values of around 0.0006 times the airfoil chord length. The flap length suited to achieve high lift gains was also identified, with the best flap efficiency obtained with flap lengths of 0.25–0.30 times the airfoil chord [7]. Figure 2 shows the blowing device obtained from this analysis and employed in the present work.

With these design choices, $C_{l,max} = 4.38$ was obtained with a jet momentum coefficient of 0.035 at a flap deflection angle of 65°.

2.2 Leading-Edge Device

The high circulation generated by the active flap dramatically reduces the stall angle of attack. This is due to the high curvature of the streamlines at the leading edge. Conventional high-lift systems employ slotted leading edge devices, slats, to address this problem. However, one of the main motivations of the present project is to find high-lift designs with potentials for noise reduction, which is pursued by avoiding the use of gaps. Following this guideline a flexible gap-less leading edge device was developed [6]. Details on the performances of the leading edge device, as well

Table 1 Aerodynamic comparison between the clean-nose airfoil and the flexible droop nose, $C_\mu = 0.035$, $Re = 12 \cdot 10^6$, $M = 0.15$

	$C_{l,max}$	$\alpha_{max}[°]$	$C_{d,stall}$	$C_{m,stall}$
Clean nose	4.46	3.0	0.071	−0.730
Droop nose	5.02	12.25	0.085	−0.729
Relative variation	+12.5 %	+9.25	+19.7 %	−0.1 %

as a comparison with a conventional slat configuration, are discussed in Ref. [8]. The local camber and the thickness were increased in the first 20 % of the airfoil chord, resulting in a reduction of the suction peak at the leading edge. The resulting aerodynamic coefficients are compared to the cruise leading-edge configuration in Table 1.

3 Numerical Approach

3.1 Flow Solver Set-Up

The flow solver employed to perform the analysis was the DLR TAU-Code [9], which uses a finite-volume approach for the solution of the Reynolds Averaged Navier-Stokes (RANS) equations. For the present study a central scheme for the spatial discretization of the mean-flow flux balance was used, while a second-order upwind Roe scheme was employed for the convective flux in the model equation representing turbulence behavior. Boundary layer transition was not taken into account, as the boundary layer was everywhere modeled as turbulent. The turbulence model of Spalart and Allmaras was employed with a correction due to flow rotation and curvature [10]. This latter module was fundamental for the simulation of the Coanda phenomenon, which is based on the equilibrium between the inertia forces and the momentum transport in the direction normal to the convex surface [11]. The numerical set-up was previously compared with wind tunnel experiments showing good accuracy [12]. The influence of additional numerical techniques and parameters is described by Thiemeier in Ref. [13].

3.2 Geometry and Grid

The aircraft geometry was the result of a preliminary overall aircraft design process performed with the PrADO software [14], Fig. 3. The wing had a sweep angle of 7°, measured on the 25 % chord line, a tapered ratio of 38 %, a twist angle of −6.94° (3.44° at the root and −3.5° at the tip), an aspect ratio of 9, and a dihedral angle of −2°. The thickness of the wing varied from 13.5 % at the root to 10.3 % at the tip.

Fig. 3 Aircraft geometry

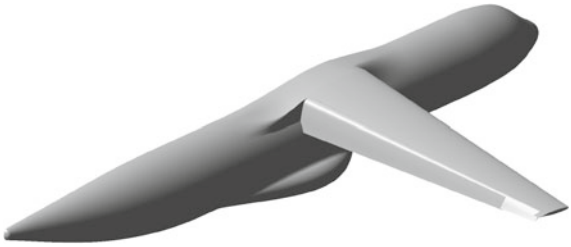

Fig. 4 Inner grid subvolumes

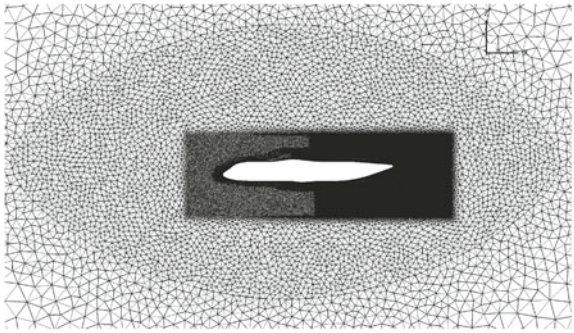

Fig. 5 Wing section grid

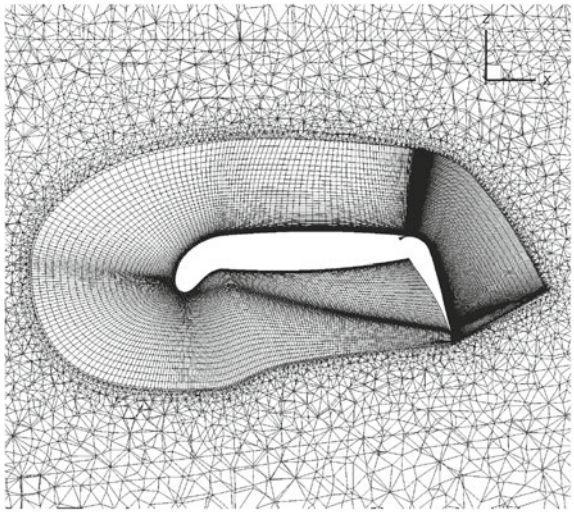

The connection between the movable surfaces and the wing were smoothed in order to facilitate the structured meshing process. A constant deflection angle of 65° was used for the flap, and 45° for the aileron, which was also equipped with a tangential blowing device.

The spatial discretization was performed by using the manual grid generator Pointwise Gridgen. Figures 5 and 6 show some sections of the volume near the model

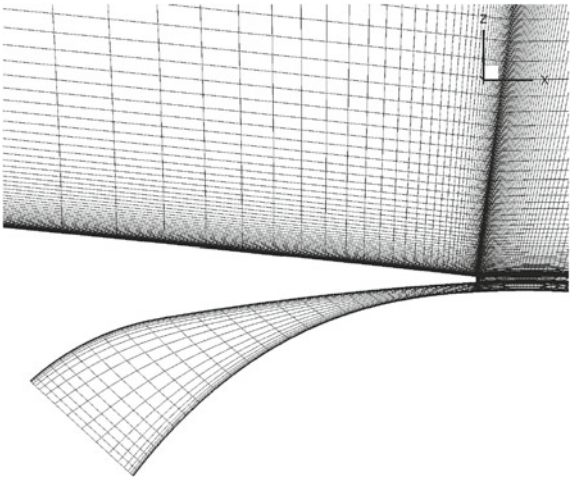

Fig. 6 Close-up of the blowing slot

surface, which was discretized by means of structured blocks. The structured volume around the wing was composed by 90 layers, 500 points in spanwise direction, and 380 points in streamwise direction. The suction side of the moving surfaces was discretized with 200 points. The volume from the inner mesh to the farfield boundaries was filled with tetrahedra, but divided into four sub-volumes, in order to adapt the grid density to the local flow conditions and the distance to the model, as shown in Fig. 4. The entire grid was made of about 50 million points, and the dimensions of the external shell were about 400 times the reference cord length, in vertical and flowstream directions, and 130 times in spanwise direction.

4 Results and Discussion

In this section the results of the RANS simulations are presented. The flow represents a typical landing phase condition, $M = 0.15$ and $Re = 12{\cdot}10^6$, based on the mean aerodynamic chord. Under these conditions, according to 2D computations, the 65° Coanda flap requires a momentum coefficient of $C_\mu = 0.035$ to provide a fully attached flow. The jet momentum is kept constant along the entire wing span, although the deflection of the aileron is reduced to 45°. This assures avoiding flow separation from the aileron at near-stall conditions, which guarantees the lateral control of the aircraft also at low speeds. Details on longitudinal stability of the present configuration are discussed by Keller in Ref. [15].

Figure 7 shows the lift development of the two tested configurations over angle of attack. As expected from the previous 2D analyses, the droop nose yields higher stall angles, leading to a significant increase of maximum lift.

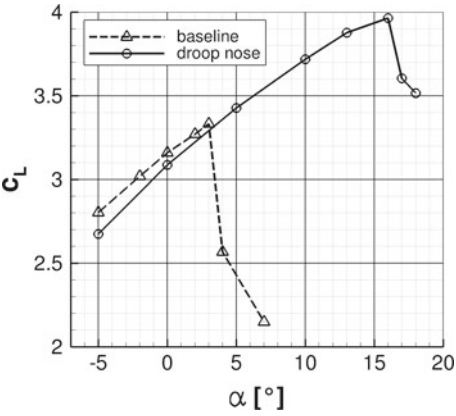

Fig. 7 Lift curves of the 3D model, droop nose and baseline configuration

The analysis that follows begins with a comparison of the airfoil performance between corresponding airfoil computations and a representative wing section of the current 3D simulation. The differences shown by the 2D versus 3D comparison are explained investigating the stall mechanisms for the two 3D leading-edge configurations.

4.1 Comparison 2D Versus 3D

An important objective of the present 3D study is the evaluation of the differences and similarities between 2D and 3D flow fields of the high-lift system. The lift and the stall angle of attack are the main parameters employed for the comparison. The airfoil analyzed to produce the present 2D data represents the section of the 3D wing in line-of-flight direction. The 3D data were obtained extracting a wing section at $\eta = 0.6$ and considering the local effective angle of attack. The local effective angle of attack differs from the global one by the local wing twist and the local downwash, which was estimated according to the lifting-line theory of Prandtl. This approach is based on the integration of the circulation along the wing, which yields an estimation of the local vertical velocity induced by the lift. The vertical velocity is then combined with the farfield velocity to estimate the local induced angle of attack. Note that this estimation is based on the assumptions of potential flow and no wing sweep angle, which are rather stretched out for the present case. The high flow curvature due to the active flap, the partial flow separation from the flap, as well as the actual lift distribution along the wing, affect the accuracy of the obtained induced angle of attack. However, the data obtained at angles of attack prior to stall can be used as basis for a comparison between the two studies, and as starting point for an analysis of the 3D simulation results.

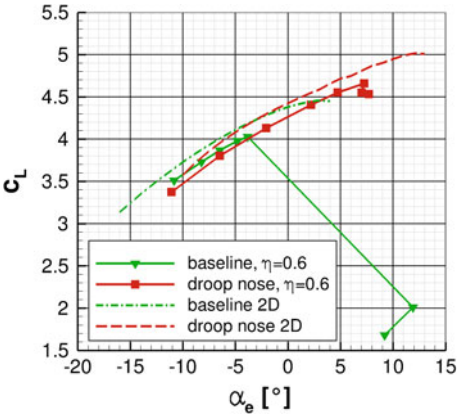

Fig. 8 Lift curves, 2D and corrected 3D-wing section, $\eta = 0.6$

Figure 8 illustrates the two lift curves for $C_\mu = 0.035$. Both the baseline and the droop nose configuration present a lower lift and a lower stall angle for the 3D case. The difference of lift coefficients between the 3D and the 2D cases within the quasi-linear range of the lift curve is about 0.2, for both configurations. The slope of the lift curves within the linear range appears very similar, which suggests that the 3D flow mechanisms do not significantly affect the generation of lift with increasing flow angle. However, the stall mechanism of the baseline configuration, a leading-edge separation starting at $\eta = 0.6$, modifies significantly the circulation distribution, making the lifting-line theory not applicable at these angles of attacks. This can be seen in Fig. 8, where the last two points of the 3D-baseline curve exhibit an unphysical behavior. In the following, sections of the 3D flows are investigated in more detail, and the causes of the disagreement between the 2D and 3D computations are explained.

4.2 Baseline Wing Configuration

Figure 9 shows the evolution of the circulation distribution in spanwise direction for different angles of attack. Until $\alpha = 3°$ the shape of the curve remains approximately constant, showing a continuous increase all along the wing. At $\alpha = 4°$ a sudden decrease of circulation takes place near the middle of the wing. The deficit of circulation extends in both directions for higher angles of attack. The aileron portion of the wing, however, remains reasonably effective, even 4° after the stall angle.

The wall streamlines and the friction coefficient contours in Figs. 11 and 12 illustrate the stall mechanism. The lift reduction is here caused by a leading-edge separation at $\eta = 0.6$ (note that the 45° aileron starts at $\eta = 0.8$). The high circulation generated by the Coanda flap creates a strong suction peak at the leading edge, which evolves in a flow separation if the flow angle is increased. It is worth mentioning

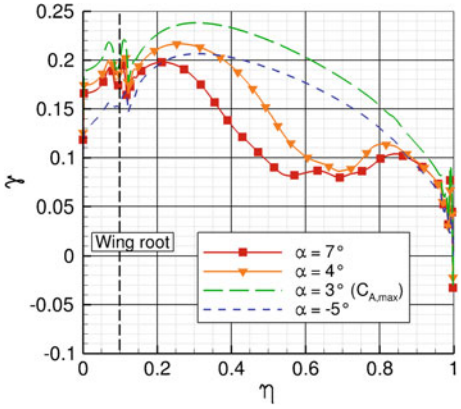

Fig. 9 Spanwise circulation distribution, baseline, $C_\mu = 0.035$

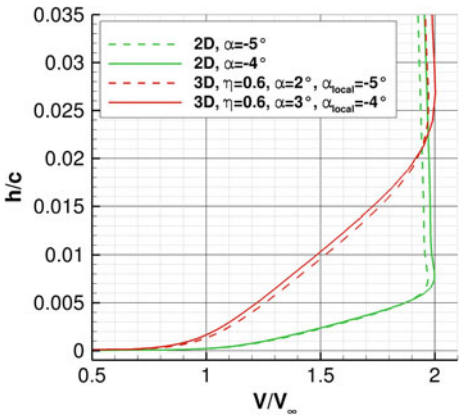

Fig. 10 Velocity profiles at 20 % chord, 2D and 3D at $\eta = 0.6$, $C_\mu = 0.035$

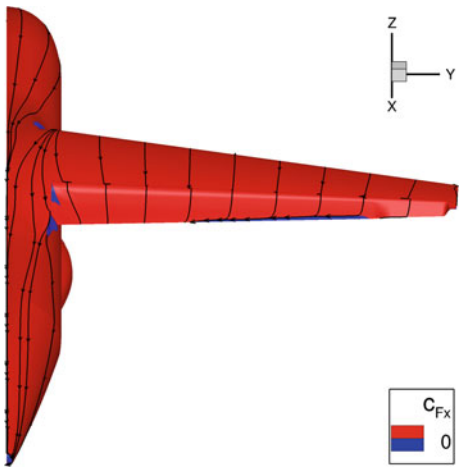

Fig. 11 Surface streamlines and longitudinal friction coefficient, baseline configuration, $\alpha = 3°$

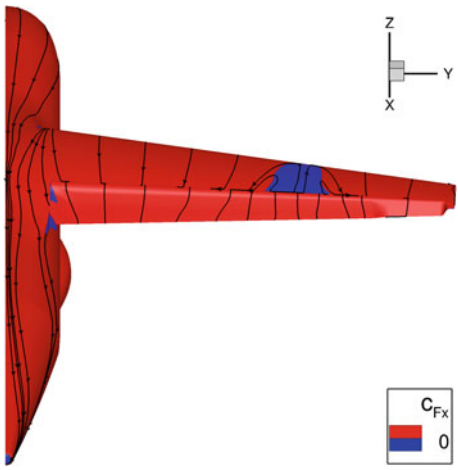

Fig. 12 Surface streamlines and longitudinal friction coefficient, baseline configuration, $\alpha = 4°$

that such a mechanism is observed in 2D computations only for C_μ higher than 0.08. For lower C_μ the reduction of lift is due to a gradual decambering of the external flow over the flap, caused by the increasing thickness of the boundary layer over the suction side of the airfoil. In this 3D case, the boundary layer along the upper side of the wing appears thicker than the 2D case, for the same C_μ and α. In Fig. 10, 2D and 3D velocity profiles are compared at the same effective angle of attack (the local twist at $\eta = 0.6$ is 1°, and the induced angle of attack is about 8°). The thicker boundary layer in the 3D case is caused by boundary layer cross flow that begins at the leading edge stagnation point, and increases with the angle of attack. For this reason, the boundary layer thickness of the outer flow increases rapidly with α. This may also explain the difference in stall angle between the 2D and 3D simulations mentioned in the previous section.

4.3 Droop Nose

As shown by the 2D analyses, the suction peak at the leading edge is significantly reduced by the droop nose. The improvement of the pressure distribution proved to prevent leading edge separation even at high jet momentum values. At these conditions, 2D stall is caused by a gradual separation between the Coanda jet and the outer flow, which causes decambering of the outer flow and reduction of lift [8]. Based on these considerations, the behavior of the 3D wing model equipped with the droop nose device is expected to be different from the baseline.

Figure 13 shows the variation of circulation distribution with the angle of attack. The distribution until the angle of maximum lift is similar to the baseline configuration, presenting the highest values at around $\eta = 0.3$ and gradually reducing towards the wing tip and root. However, the reduction of circulation caused by wing

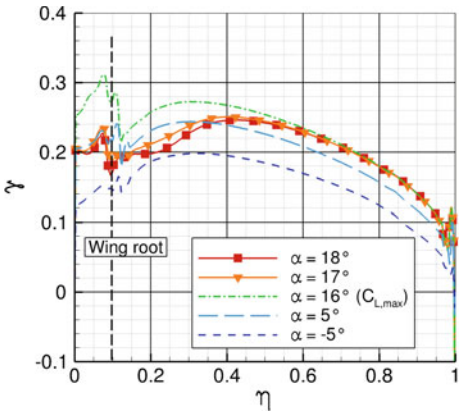

Fig. 13 Spanwise circulation distribution, droop nose, $C_\mu = 0.035$

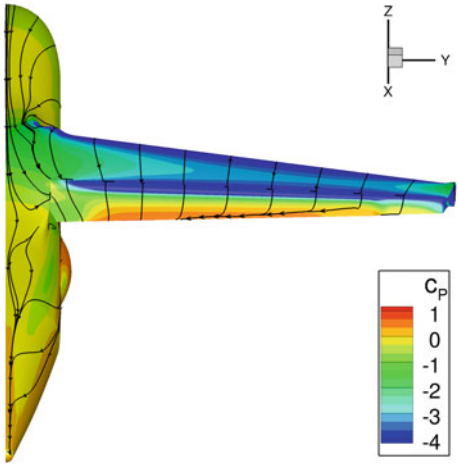

Fig. 14 Surface streamlines and C_p distribution, droop nose, $\alpha = 16°$

stall appears in the proximity of the wing root, whereas the outer half of the wing maintains attached flow. This behavior can be explained by looking at the surface streamlines and pressure coefficient distributions.

Figures 14 and 15 show the evolution of the flow near the model surface close to wing stall. A trailing-edge flow separation is visible in the outer half of the flap area, but it does not seem to vary significantly during stall. On the other hand, the pressure coefficient at the wing root presents substantial variations. For an increase of angle of attack of 1°, the suction peak on the Coanda surface is dramatically reduced, until $\eta = 0.3$. In the same area, the surface streamlines show a strong cross flow which directs near-wall fluid from the fuselage to the Coanda flap, over the suction side of the wing. For alpha higher then 16°, the strong suction over the wing increases the cross flow, which thus reaches the Coanda flap. Under these conditions, the thick boundary layer developed along the fuselage affects the efficiency of the Coanda flap.

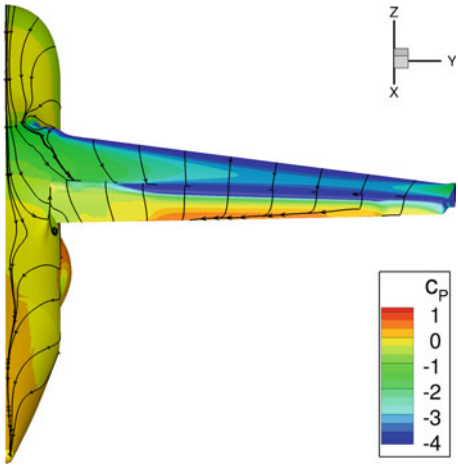

Fig. 15 Surface streamlines and C_p distribution, droop nose, $\alpha = 17°$

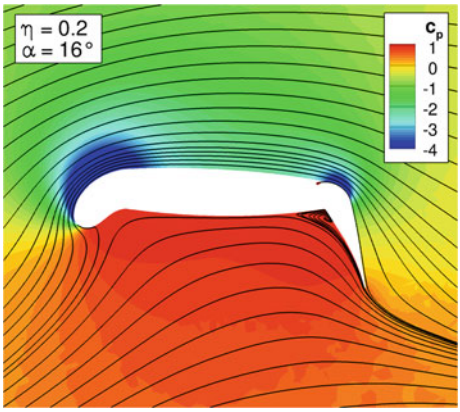

Fig. 16 Streamlines and C_p distribution, $\eta = 0.2$, $\alpha = 16°$

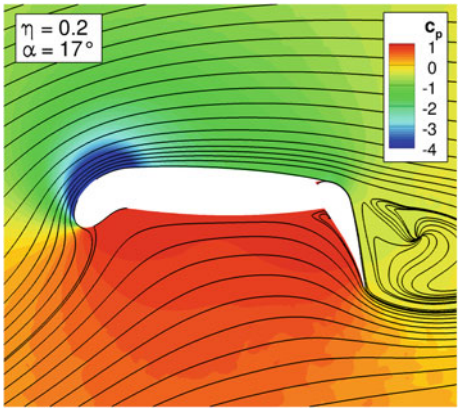

Fig. 17 Streamlines and C_p distribution, $\eta = 0.2$, $\alpha = 17°$

The consequences of the thick boundary layer on the Coanda flap are illustrated in Figs. 16 and 17, which show the flow field at $\eta = 0.2$ at maximum lift and just after stall. Until the stall angle, an increase of α generates stronger suction over the droop nose without causing separation. However, 1° after stall the outer flow is completely separated from the Coanda jet, which remains attached to the flap surface. As a consequence, a large recirculation area occurs downstream of the flap, and the outer flow turning is dramatically reduced.

5 Conclusion

The integration of an active circulation control configuration into a 3D high-wing aircraft model was carried out in order to assess the design of the high-lift system previously performed by means of 2D simulations. The trailing edge of the wing was equipped with a simple-hinged flap deflected by 65° for the flap and 45° for the aileron. Flow separation from the deflected surface was avoided by tangential blowing. In combination to the trailing edge active flap, two leading-edge geometries were tested, the cruise configuration and a gap-less flexible droop nose device.

3D flow affected the behavior of the Coanda flap already within the linear range of the lift curve. The main cause of the observed loss of lift coefficient of around 0.2, was assumed to be boundary layer cross flow at the wing leading edge. This increased the viscous losses of the flow that reached the Coanda flap and reduced the effect of the wall jet to achieve flow turning. This mechanism was also responsible for the early leading edge stall observed with the cruise leading-edge configuration. In this case, stall occurred at $\alpha = -3°$, which is about 6° less than observed with 2D analyses. The lift and stall angle improvements yielded by the droop nose were similar to the ones emerged from the 2D studies, although the stall mechanism was different in the case of droop nose. Due to the low pressure over the wing, a strong cross flow from the fuselage to the wing appeared at the wing root for angles of attack above 16°. This caused a thick boundary layer to reach the Coanda flap, causing a separation between the jet and the outer flow and resulting in a sudden reduction of lift.

The present work highlighted the importance of avoiding adverse 3D boundary layer flow effects in suited integrations of an active high-lift system on a high-wing aircraft configuration.

Acknowledgments The funding of this work of the Collaborative Research Centre SFB 880 by the German Research Foundation, DFG, is thankfully acknowledged.